Published in final edited form as:

Nature. 2020 May ; 581(7807): 194–198. doi:10.1038/s41586-020-2204-1.

Retinal innervation tunes circuits that drive nonphotic entrainment to food

Diego Carlos Fernandez[1], **Ruchi Komal**[1], **Jennifer Langel**[1], **Jun Ma**[1], **Phan Q. Duy**[1,2], **Mario A. Penzo**[1], **Haiqing Zhao**[3], **Samer Hattar**[1]

[1]National Institute of Mental Health (NIMH), National Institutes of Health (NIH), Bethesda, MD 20892, USA

[2]Current Address: MSTP, Yale University, New Haven, CT 06520, USA

[3]Department of Biology, Johns Hopkins University, Baltimore, MD 21218, USA

Abstract

Daily changes in light and food availability are major time-cues influencing circadian timing[1]. Little is known, however, about the circuits integrating these time-cues to drive a coherent circadian output[1–3]. Here, we investigated whether retinal inputs modulate the entrainment to non-photic cues, such as time-restricted feeding. Photic information is relayed to the suprachiasmatic nucleus (SCN), which houses the central circadian pacemaker, and the intergeniculate leaflet (IGL) through intrinsically-photosensitive retinal ganglion cells (ipRGCs)[4]. Adult mice lacking ipRGCs since early-postnatal stages displayed impaired entrainment to time-restricted feeding, whereas ablating ipRGCs at later stages had no effect. Early-postnatal ipRGC innervation influences neuropeptide Y (NPY)-expressing IGL neurons, guiding the functional IGL^{NPY}-SCN circuit assembly. Moreover, silencing the IGL^{NPY} neurons in adult animals mimicked the deficits induced by early-postnatal ipRGC ablation, and acute inhibition of IGL^{NPY} terminals in the SCN decreased food-anticipatory activity. Thus, early-postnatal ipRGC innervation tunes the IGL^{NPY}-SCN circuit to allow entrainment to time-restricted feeding.

The circadian system is composed of a central circadian pacemaker, housed in the suprachiasmatic nucleus (SCN), which orchestrates rhythmic functions of peripheral clocks located throughout the body[1]. This system integrates multiple time-cues from the sensory, as

Co-corresponding authors: Samer Hattar, samer.hattar@nih.gov, Diego Carlos Fernandez, diego.fernandez@nih.gov.

AUTHOR CONTRIBUTIONS

DCF: Conceptualization, formal analysis, investigation, methodology, project administration, supervision, visualization and writing (original draft & editing); RK: investigation, methodology, and writing (review & editing). JL: investigation, methodology, and writing (review & editing). JM: investigation, methodology, and writing (review & editing). PQD: investigation, and methodology. MP: Funding acquisition, writing (review & editing). HZ: Funding acquisition, writing (review & editing). SH: Conceptualization, funding acquisition, project administration, supervision, and writing (original draft & editing).

DATA AVAILABILITY

The principal data supporting the findings of this work are available within the figures and the Supplementary Information. Additional data that support the findings of this study are available from the corresponding authors on request.

COMPETING INTERESTS

Authors declare no competing interests.

well as the circadian and metabolic systems to generate a coherent perception of the environment[2,3]. At present, little is known about the brain circuits and mechanisms that integrate different time-cues to drive a coordinated circadian output.

In mammals, light is transmitted to circadian centers through a subpopulation of retinal ganglion cells (RGCs)[4] that are intrinsically photosensitive (ip) due to the expression of the photopigment melanopsin (*Opn4*)[5,6] to drive circadian photoentrainment. As a central pacemaker, the SCN receives dense axonal projections from multiple brain areas, particularly the thalamic intergeniculate leaflet (IGL), thought to be involved in the circadian entrainment to non-photic cues (non-photic entrainment)[7–10]. Here, we show that retinal input impacts circadian circuits that control non-photic entrainment.

RESULTS

ipRGC ablation attenuates timed feeding

We assessed the impact of ablating retinal input on circuits controlling entrainment to non-photic time-cues. We used a mouse line that removes ipRGCs during development to early postnatal stages through the expression of diphtheria toxin A subunit (*Opn4*^{DTA} mice)[11]. Non-photic entrainment was evaluated by limiting the food access to a 7-hour time window (Fig. 1a), in what is known as time-restricted feeding (TRF)[12]. We opted to keep animals under constant darkness (DD), thus the time-restricted access to food constitutes the only recurrent time-cue for mice. Both female and male control and *Opn4*^{DTA} mice with food *ad libitum* (free-running conditions) showed robust rhythmic patterns of feeding that closely overlap with their locomotor activity patterns (Extended data Fig. 1a-b), confirming that early ipRGC ablation has no effects on locomotor activity and rhythmic feeding pattern in adult mice.

Under TRF, control mice displayed a robust and sustained food-anticipatory activity (Fig. 1b-d and Extended data Fig. 1c)[13,14]. *Opn4*^{DTA} mice showed deficits in the non-photic entrainment to TRF (Fig. 1b-d and Extended data Fig. 1d), as reduced food-anticipatory activity was observed throughout the restriction paradigm (Fig. 1e-f). A graded-score analysis system (see methods section for a full description and Extended data Fig. 1e) similarly showed significant deficits in the circadian anticipation to TRF in mice lacking ipRGC innervation (Fig. 1g).

We next evaluated hormones involved in feeding control. Levels of insulin, leptin, and total ghrelin, as well as glucose, were similar in control and *Opn4*^{DTA} mice under free-running conditions (Extended data Table 1). Under TRF, control and *Opn4*^{DTA} mice had similar levels of glucose and anorexigenic hormones, leptin and insulin (Fig. 1h-i and Extended data Table 1). In addition, control and *Opn4*^{DTA} mice consumed similar amount of food and their feeding patterns, body weight, and body composition were indistinguishable (Extended data Fig. 1f-j). Together, these results indicate that the behavioral alterations observed in mice lacking ipRGCs are not caused by changes in food intake or caloric restriction.

The levels of total ghrelin, an orexigenic hormone known for its stimulatory effects on food intake[15,16], were increased in anticipation to food in control, but not in *Opn4*^{DTA} mice (Fig.

1j and Extended data Table 1). The differences in total ghrelin levels between groups were observed as early as day 7 after TRF and persisted throughout (Extended data Fig. 1k). These results indicate that the lack of anticipatory ghrelin responses in *Opn4*^{DTA} mice correlate with the impaired anticipatory activity to timed feeding.

ipRGCs influence the IGL-SCN circuit

Several brain and peripheral areas exhibit changes in activity in response to TRF[17]. The reduced non-photic entrainment displayed by *Opn4*^{DTA} mice suggests the involvement of an ipRGC target. The intergeniculate nucleus (IGL) receives dense ipRGC innervation and is implicated in driving photic and non-photic signals to modulate circadian processes[7,18]. Indeed, we found that mice exposed to TRF showed a substantial induction of the immediate-early gene, *c-Fos*, in IGL neurons (Fig. 2a-c). *Opn4*^{DTA} mice exposed to the same paradigm, however, showed a reduced c-Fos induction in the IGL (Fig. 2b-c). Importantly, in control and *Opn4*^{DTA} mice, c-Fos induction was not observed in the hypothalamic arcuate nucleus, an area known to be involved in the homeostatic control of hunger and food intake[19] (Extended data Fig. 2a-c). These results implicate the IGL as a brain region involved in circadian entrainment to TRF.

The IGL contains neurons expressing neuropeptide Y (NPY) that project to SCN[7–9]. To better characterize the innervation pattern of IGL^{NPY} neurons, we injected a cre-dependent adeno-associated virus (AAV)-DIO-tdTomato in the IGL of *NPY*$^{cre/+}$ mice. We found that IGL^{NPY} neurons innervate both the ipsi- and contralateral SCN, and to a lesser extent, send unilateral projections to other brain regions (Extended data Fig. 2d-h). Early ipRGC ablation causes a significant reduction in the NPY-immunoreactivity in IGL neurons (Fig. 2d-e), whereas the number of NPY(+) somas and DAPI nuclei were unaffected (Fig. 2f-g). Consistent with the reduction in NPY levels in the IGL, we also found a significant reduction in NPY(+) reactivity in the SCN of *Opn4*^{DTA} mice (Fig. 2h-j, Extended data Fig. 2i-j, and Supplementary Videos 1-2). However, when we correlated the NPY levels from the SCN and the IGL, we found that the NPY staining in the IGL covers a larger percentage of the leaflet compared to the SCN nuclei in *Opn4*^{DTA} mice (Extended data Fig. 2j), suggesting that NPY axonal transport could also be affected. Non-ipRGC innervated structures that express high levels of NPY showed normal patterns of NPY-immunostaining (Extended data Fig. 2k).

Time window for IGL-SCN circuit assembly

We next evaluated whether ipRGC ablation at adult stages causes similar alterations. We used a mouse line expressing an attenuated form of the diphtheria toxin (attnDTA, also known as aDTA) controlled by the melanopsin promoter (*Opn4*^{attnDTA}), inducing the ipRGC ablation only by 6 months of age[4]. Eliminating the ipRGC innervation in adult mice had no significant effect on NPY levels in fibers innervating the SCN (Fig. 3a-b). In addition, adult *Opn4*^{attnDTA} mice exposed to the TRF protocol showed robust food-anticipatory activity, comparable to age-matched controls (Fig. 3c-e and Extended data Fig. 3a-b). These results indicate that ipRGC innervation plays an important role over circuits controlling entrainment to TRF specifically during early postnatal stages.

To determine the critical period for the influence of ipRGC innervation on IGL^{NPY}-SCN circuit assembly and non-photic entrainment, we enucleated WT animals at different postnatal stages. We found that the IGL^{NPY}-SCN circuit was disrupted in adult mice that were enucleated at postnatal day (P) 0 to early adulthood stages (P40). However, enucleation of mice at later adulthood stages (P90) had no significant effect (Fig. 3f-g, Extended data Fig. 3c, and Supplementary Videos 3-6). Concordantly, WT mice enucleated at P0 and P40 showed significant deficits in the entrainment to TRF, while P90 enucleated mice displayed robust food-anticipatory responses (Fig. 3h-l and Extended data Fig. 3d-g). These results indicate that there is a critical time window for ipRGC innervation to influence the IGL^{NPY}-SCN circuit assembly and non-photic entrainment.

ipRGC-SCN axons regulate IGL-SCN circuit

SCN and IGL receive dense ipRGC input[8,9], suggesting that ipRGCs could directly affect IGL^{NPY} neurons, their axonal projections at SCN level, or a combination of both. To test these possibilities, we used a mouse line (*Opn4*$^{Cre/+}$;*Brn3b*$^{DTA/+}$) in which *Brn3b*(−) ipRGCs innervating the SCN survive (Extended data Fig. 4a), while *Brn3b*(+) ipRGCs mostly projecting to non-SCN regions (including the IGL) are ablated during early postnatal stages[20,21]. In *Opn4*$^{Cre/+}$; *Brn3b*$^{DTA/+}$ mice, NPY immunostaining was unaffected in both the IGL and SCN (Extended data Fig. 4a-c), and these animals showed sustained food-anticipatory activity to TRF (Extended data Fig. 4d-h). Thus, ipRGC innervation to the SCN is sufficient for tuning the functional assembly of the IGL^{NPY}-SCN circuit.

ipRGCs establish NPY levels in IGL

The reduced NPY levels in fibers innervating the SCN suggest that there is either a drastic depletion of the neuropeptide or a lack of axonal innervation from IGL. To test this, *NPY*$^{cre/+}$ mice were enucleated at P0 and three months later mice were injected in the IGL with a cre-dependent AAV to trace NPY(+) projections and their synaptic terminals (Extended data Fig. 5a-b). We found that the innervation pattern and the density of synaptic terminals at SCN level were not affected in adult *NPY*$^{cre/+}$ mice that were enucleated at P0 (Extended data Fig. 5c-d), demonstrating that early ipRGC ablation affects NPY levels, but not IGL^{NPY} axonal projections.

IGL^{NPY} neurons affect entrainment to TRF

Adult mice lacking NPY (NPY KO) showed reduced entrainment to TRF (Extended data Fig. 6a-d). In addition, NPY KO mice showed a reduction in the amount of food consumed during the TRF paradigm (Extended data Fig. 6e), reflecting the critical role that NPY signaling plays in overall feeding behavior[22].

To silence IGL^{NPY} neurons synaptic release, a cre-dependent AAV encoding tetanus toxin light chain subunit (TenT)-GFP was injected in adult *NPY*$^{cre/+}$ mice (Fig. 4a). AAV/DIO-GFP-injected *NPY*$^{cre/+}$ mice were used as control group. Injection sites were confirmed *post hoc* by assessing GFP expression (Fig. 4a). Four weeks after AAV-injections, mice were exposed to the TRF paradigm. The inhibition of synaptic release specifically in IGL^{NPY} neurons abolished the food-anticipatory activity (Fig. 4b-f and Extended data Fig. 6f-g). It is important to note that, similar to NPY KO animals, the amount of food consumed by

NPY$^{cre/+}$ mice was also reduced when housed with access to food *ad libitum* (Extended data Fig. 6e). However, this reduction was further exacerbated in AAV/TenT-injected *NPY*$^{cre/+}$ mice during the time-restricted access to food (Extended data Fig. 6e).

To specifically manipulate the IGL^{NPY}-SCN circuit, we used a virally delivered optogenetic strategy to transiently silence IGL^{NPY} projections innervating the SCN. A cre-dependent AAV/DIO-ArchT-tdTomato (ArchT, archaerhodopsin TP009) was bilaterally injected in adult *NPY*$^{cre/+}$ mice (*NPY*$^{cre/+}$-ArchT), and optical fibers were implanted just above the SCN (Fig. 4g). As control group, *NPY*$^{cre/+}$ mice were injected with an AAV/DIO-tdTomato (*NPY*$^{cre/+}$-sham; Extended data Fig. 7a). Mice were allowed to recover for 2 weeks, and then placed under TRF. Both *NPY*$^{cre/+}$-sham and *NPY*$^{cre/+}$-ArchT mice showed similar food-anticipatory activity and food consumption (Extended data Fig. 7b-d). Next, the neural silencing was optogenetically induced in the IGL^{NPY}-SCN circuit starting two hours before food delivery, by applying 3 pulses of 20 min of light, with 20 min intervals (Fig. 4h). Locomotor activity was measured starting 3 hours before food delivery, and the total activity recorded before and after neuronal silencing was compared in both groups of mice. Control *NPY*$^{cre/+}$-sham mice displayed no significant changes in the locomotor activity (Fig. 4i and extended data Fig. 7e, g-h). In contrast, *NPY*$^{cre/+}$-ArchT mice displayed reduced exploratory activity during the optical silencing of NPY$^{ArchT(+)}$ fibers (Fig. 4j and extended data Fig. 7f-h), without affecting subsequent feeding behavior (Extended data Fig. 7c-d). These results demonstrate that the signaling of IGL^{NPY} neurons projecting specifically to SCN is required for entrainment to TRF.

DISCUSSION

Here we reveal that early ipRGC innervation impacts the IGL^{NPY}-SCN functional circuit assembly. Moreover, the correct assembly of this circuit is necessary for circadian anticipatory responses associated with TRF in adult mice.

Integration of environmental cues occurs widely in the nervous system. It has been extensively documented that early ablation of retinal input to the superior colliculus, a major node of multi-sensory integration[23], leads to an extensive rewiring of its sensory inputs[24], causing the strengthening of responses to non-visual stimuli[25,26]. Based on these results, our original expectation was that ablating ipRGC innervation to brain centers would cause a strengthening of circadian entrainment to non-photic modalities. Our results show a weakening of non-photic entrainment in mice lacking early retinal innervation to brain targets. Therefore, we propose that the retina-IGL^{NPY}-SCN circuits do not follow the conventional model of early plasticity described for the image-forming visual system.

Feeding behavior is the result of the integration of multiple responses to food, including energy homeostasis[27], hedonic reward[28] and memory traces[29], as well as anticipation to timed food availability driven by a food-entrainable oscillator (FEO)[30,31]. Our results suggest that IGL^{NPY} neurons require retinal innervation to the SCN during early development for normal circuit assembly, and act as a node of connection between the FEO network and the central pacemaker (SCN) in adult animals (Extended data Fig. 8 and supplementary discussion).

MATERIALS AND METHODS

Animals

Female and male mice were used in this study. Wild-type (WT) mice of a mixed background (B6/129 F1 hybrid, Stock #101043), *NPY*^{tm1Rpa} (Stock #4545), and *NPY*^{cre} (Stock # 27851) mice were obtained from the Jackson Laboratory. *Opn4*$^{DTA/DTA}$, *Opn4*$^{attnDTA/attnDTA}$, and *Opn4*$^{Cre/+}$;*Brn3b*$^{DTA/+}$ mouse lines were previously described[4,11,20,21]. All animals were handled in accordance with guidelines of the Animal Care and Use Committees of the National Institute of Mental Health (NIMH). All efforts were made to minimize the pain and the number of animals used.

Locomotor and feeding activity measurements

Mice were housed under a 12 h:12 h light/dark cycle (T24) or constant darkness (DD) at a temperature of 22°C. During all the behavioral experiments mice were single-housed. General locomotor activity was monitored using infrared motion detectors from Mini Mitter (Respironics) mounted on top of the cages. Data was collected in 5-min bins using Vital-View software (Mini Mitter). Feeding activity was monitored using programmable feeders (Actimetrics), as previously described[32]. ClockLab (Actimetrics) software was used to set the TRF schedules, and to measure number of pellets consumed. Dustless Precision Pellets were used (300 mg pellets; Bio-Serv; product #F0170). Actograms, total activity, periodograms, and period lengths were obtained and calculated using ClockLab (Actimetrics).

The locomotor activity (9 hours) before food access was measured and results were expressed as percentage of activity relative to total locomotor activity; the area under the curve was analyzed for both all animals.

Food-anticipatory activity (FAA) was determined as: locomotor activity measured 3 hours before food access relative to the total activity during the TRF protocol.

When exposed to DD with food *ad libitum*, we observed that some genetic mouse lines displayed different free-running periods. Therefore, we implemented a graded-score analysis to account for potential variations in the food-anticipatory activity caused by differences in the free-running periods displayed before and during the TRF paradigm. The analysis was performed with the experimenter blind to genotype and/or condition. Entrainment to TRF was graded on a scale from 0 to 5: ***Score 0*** indicates no FAA defined as less than 5% of total activity, with unperturbed free-running locomotor activity defined as less than 15 min change in period length. ***Score 0.1 – 1*** indicates no FAA defined as less than 5% of total activity with changes in the free-running locomotor activity defined as more than 15 min change in period length. ***Score 1.1 – 2*** indicates a weak or sporadic FAA defined as less than 10% of total activity, and with or without changes in free-running locomotor activity. ***Score 2.1 – 3*** indicates a sustained FAA of 10 – 15% of total activity with or without changes in free-running locomotor activity. ***Score 3.1 – 4*** indicates robust FAA defined as more than 15% of total activity and unperturbed free-running locomotor activity defined as less than 15 min change in period length. ***Score 4.1 – 5*** indicates robust FAA defined as more than 15%

of total activity with changes in the free-running locomotor activity defined as more than 15 min change in period length.

Retinal injections

Retinal projections were visualized using intravitreal injections (1 μl) of the tracer cholera toxin b-subunit (CTB) fluorescently conjugated (Alexa Fluor 488 or 594, Thermofisher). Mice were anesthetized using isoflurane and placed under a stereo-microscope. The microscope and all the instruments were properly cleaned and sterilized. A glass needle (pulled 10 μL microcapillary tube, Sigma P0674) and a 10 μL Hamilton syringe were used to drive the solution into the vitreous chamber of the eye to ensure delivery specifically to the retina. After slowly injecting the total volume, pipette was left in place for 60–90 sec. Mice recovered from injections on a heating pad until they woke from anesthesia. After injections, animals were given 3 to 4 days recovery period. Finally, mice were deeply anesthetized, and perfused intracardially with 4% paraformaldehyde (Electron Microscopy Sciences). Brains were post-fixed overnight in the same fixative, and coronal brain sections were obtained using a cryostat.

Stereotaxic injections and optical fibers implantation

The stereotaxic frame and all instruments were properly cleaned and sterilized. Mice were deeply anesthetized using isoflurane as confirmed by complete absence of flinching response to pinch. Skull fur was shaved, the head of the mouse was then fixed to the stereotaxic frame, cleaned by scrubbing with povidone-iodine and 70% ethanol and the skull was exposed using a sterile scalpel. A small hole was drilled over the region of interest. Coordinates follow the Paxinos and Franklin mouse atlas[33]. For IGL injections, the following coordinates were used: –4.21 mm from Bregma, ±2.45 mm lateral from midline, and −2.30 mm vertical from cortical surface. AAV injections were performed using a microinjector (Nanojector II, Drummond Scientific Company) and pulled 10 μL microcapillary pipettes. During the entire procedure, a heating pad was used to maintain stable body temperature in mice. At the end of the surgical procedure, the incision was closed using nylon sutures. Systemic analgesics (either buprenorphine, 0.1 mg/kg, or Meloxicam, 1 mg/kg) were administrated before and after surgery.

For anatomical analysis, AAVs (AAV2/9-phSyn1(S)-Flex-tdTomato-T2A-SynEGFP-WPRE obtained from Boston Children's Hospital Viral Core with a titer of 4.26×10^{13} Genome Copies (GC)/ml and AAV5/Syn-DIO-hChR2(H134R)-EGFP-WPRE-HGHpA obtained from Addgene #20298 with a titer of 1×10^{13} GC/ml) were used. Mice were perfused at different times post-injection and the brains were subsequently sectioned on a cryostat.

For silencing NPY IGL neurons, AAVs (AAV5/Syn-DIO-hChR2(H134R)-EGFP-WPRE-HGHpA obtained from Addgene #20298 with a titer of 1×10^{13} GC/ml (control), and pAAV5/CMV-DIO-eGFP-2A-TeNT, GVVC-AAV-71 (TeNT) obtained from Stanford University #2237 with a titer of 1×10^{13} GC/ml) were used. Mice were then tested for time restricted feeding.

For optogenetic experiments, AAVs (AAV5/DIO-tdTomato (control for the optogenetic virus) and AAV5/DIO-ArchT-tdTomato obtained from Addgene) were bilaterally injected

into the IGL. A week after virus injections, optical fibers (100 μm diameter, Thorlabs) were implanted above the SCN (–0.50 mm from Bregma, ±0.15 mm lateral from midline, and −5.60 mm vertical from cortical surface, 9.99° angle) and were affixed to the skull using Metabond Cement System (Parkell, Inc.) and Jet Brand dental acrylic (Lang Dental Manufacturing Co., Inc.). Following all surgical procedures, animals recovered on a heating pad and returned to their home cages after 24 h post-surgery recovery and monitoring. Animals received subcutaneous injections of meloxicam (1–2 mg/kg) for analgesia and anti-inflammatory purposes. 2 weeks after recovery under light/dark cycle, mice were exposed to TRF for 3–4 weeks.

The optical fibers were connected to a laser source (Ce:YAG, Ce:YAG & LED Driver, Doric Lenses) via a dual fibre rotary joint (FRJ_1×2i_FC-2FC; Doric Lenses) using an optic fibre sleeve (Thorlabs). The light intensity at the interface between the fiber tip and the animal was 10 mW. Optical stimulation was delivered two hours before food delivery, by applying 3 pulses of 20 min of light, with 20 min intervals. Mice without correct targeting of tracers and/or vectors were excluded from this study.

Eye enucleation

P0 mice were deeply anesthetized, and a ~1 mm incision was made across each eyelid using a sterile scalpel. Finally, sterilized forceps were used to pull the eyes free of the orbitals. For adult mice enucleation, animals were deeply anesthetized and a sterile curved scissor was used to cut the optic nerve and remove both eyes. Bleeding was controlled by orbital pressure on the eye with a sterile cotton swab. Before and after surgery, systemic analgesics (buprenorphine, 0.1 mg/kg) were administrated. Animals were monitored over the next several days for signs of infection.

Immunofluorescence

Brain sections were incubated in 0.1M PBS with 3% Goat serum (Vector Labs) and 0.3% Triton X-100 (Sigma-Aldrich) for 2 hours, and then incubated using the following antibodies (overnight, at 4°C): rabbit α-RFP (MBL PM005, 1:1000); chicken α -GFP (AbCam Ab13970, 1:2000); mouse IgG1 α-c-Fos (EnCor MCA-2H2, 1:1000); rabbit antibody α -NPY (Peninsula lab T-4070, 1:500). After several washing steps, Alexa-conjugated secondary antibodies were used (Molecular Probes, 1:500, for 2 hours at room temperature). Finally, slides were mounted using AntiFade medium (Molecular Probes). Images were acquired using an Eclipse Ti2 confocal microscope (Nikon).

Quantification and statistical analysis

For all morphometric image processing, digitalized captured TIF-images were assembled and processed with NIS Elements (Nikon) Version 5.02 and Adobe Photoshop (Adobe Systems), and transferred to ImageJ software (NIH, USA). Sample analysis was performed with the experimenter blind to condition. All the nomenclature used in the manuscript follows that of Paxinos & Franklin Atlas[33].

IGL/arcuate nucleus morphometric analysis

Total IGL or arcuate nucleus areas of analysis were manually outlined in coronal brain sections based on DAPI staining. Bilateral nuclei were evaluated per section.

c-Fos induction: Mice were exposed to the TRF paradigm for 3 weeks. On the 21st day mice were perfused right before the time of food delivery. As control group, mice with food *ad libitum* were perfused at circadian time (CT) 11–12 (before activity onset). In all cases, mice were under DD conditions. c-Fos(+) cells were manually counted in the delineated IGL or arcuate nucleus area, and results obtained from 5–6 separate coronal sections were averaged per animal.

NPY levels: Mice housed under T24 cycle were perfused at CT 14–16. Digital images were converted to 8-bits gray scale, and the optic density indicating NPY expression levels in the IGL were measured. For measuring number of NPY(+) neurons in the IGL, a 3D reconstruction was obtained from *z*-stack images (15–20 μm), which were overexposed (to account for different NPY expression levels) and the number of NPY(+) somas were manually counted. Finally, the number of DAPI(+) nuclei were manually counted. In all cases, results obtained from 5–6 separate coronal sections were averaged per animal.

SCN morphometric analysis

Total SCN area of analysis was manually outlined in coronal brain sections based on DAPI staining. Digital images were converted to 8-bits gray scale, and the optic density indicating NPY expression or Syn-GFP levels were measured. Results obtained from 3–6 separate coronal sections were averaged per animal.

Metabolic measurements

Anorexigenic and orexigenic hormones were measured by ELISA. Blood samples were collected and stored in EDTA-coated tubes (BD Microtainer 365974). Plasma was then obtained, and ghrelin (total), insulin, and leptin levels were measured using the following ELISA kits: rat/mouse total ghrelin (Millipore EZRGRT-91K); rat insulin (Crystal Chem 90010); mouse leptin (R&DSystems MOB00). Blood glucose was measured using a regular blood glucometer. Samples were taken from the mice tails, under dim red light.

Body composition was measured in awake animals using quantitative magnetic resonance technology (EchoMRI composition analyzer).

Statistical Analysis

Calculation of sample size per experiment was determined, or confirm by post hoc analyses, using a G*Power 3 software[34,35].

Statistical analysis of results was made by using Student’s t test (parametric or non-parametric (Mann-Whitney)), or analysis of variance (ANOVA), followed by Tukey’s or Sidak’s multiple comparisons tests, as stated. All the analyses were done using GraphPad Prism, version 7.0a.

Extended Data

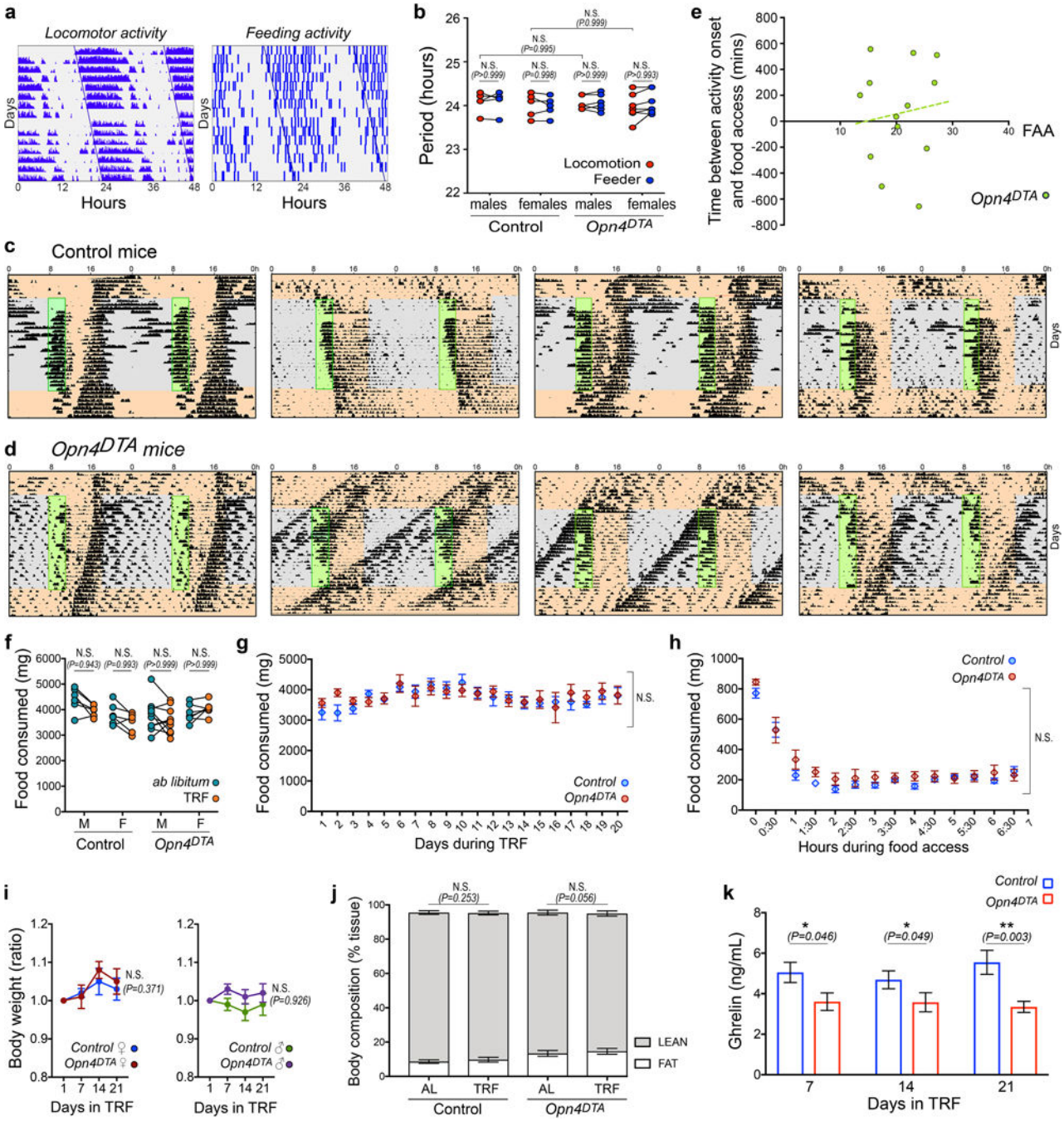

Extended data Fig. 1. Early ipRGC ablation alters the entrainment to time-restricted feeding.

(**a** and **b**) General locomotor activity and feeding behavior were monitored using infrared sensors and programmable feeders, respectively. Representative actograms obtained from an *Opn4*^{DTA} mouse under free-running (DD and food *ad libitum*) are shown (**a**). Periodograms were obtained, and no differences in period lengths were found between locomotor activity and the feeding behavior for both groups (**b**). Data are mean ± SEM (n = 12 mice), two-way ANOVA, followed by Sidak's multiple comparisons test.

(**c** and **d**) Representative actograms obtained from control (**c**) and *Opn4*^{DTA} (**d**) mice exposed to time-restricted feeding (TRF) are shown.

(**e**) Under constant darkness and food *ad libitum*, *Opn4*^{DTA} mice displayed different free-running periods. Therefore, we analyzed whether there is any correlation between the food-anticipatory activity (measured during a 3h time window) and the time difference (measured in minutes) between the onset of locomotor activity and the time of food delivery measured during the first day of food restriction. No significant correlations (*Pearson* correlation test, $P = 0.6379$) were observed in *Opn4*^{DTA} mice (n = 13 mice).

(**f**) The daily total amount of food consumed was measured in male (M) and female (F) control and *Opn4*^{DTA} mice exposed to free-running (food *ad libitum*) or TRF paradigm. Data are mean ± SEM (n = 8 mice), two-way ANOVA, followed by Sidak's multiple comparisons test.

(**g**) Total food consumption per day during TRF. Data are mean ± SEM (n = 8 mice), multiple Student's t test, two tailed.

(**h**) Pattern of food consumption during the 7 hours of food access. Data are mean ± SEM (n = 8 mice); multiple Student's t test, two tailed.

(**i**) Measurement of the body weight of female and male mice exposed to the TRF paradigm. Data are mean ± SEM (n = 12 mice), two-way ANOVA, followed by Sidak's multiple comparisons test.

(**j**) The body composition was measured in mice with food *ad libitum* (AL), or on the 21st day of TRF. Data are mean ± SEM (n = 8 mice), two-way ANOVA, followed by Sidak's multiple comparisons test.

(**k**) Total ghrelin levels (ng/mL) were measured in control and *Opn4*^{DTA} mice after 7, 14, and 21 days of TRF. In all cases samples were collected right before food delivery. Data are mean ± SEM (n = 8 mice), Student's t test, two tailed.

TRF: time-restricted feeding; FFA: food-anticipatory activity.

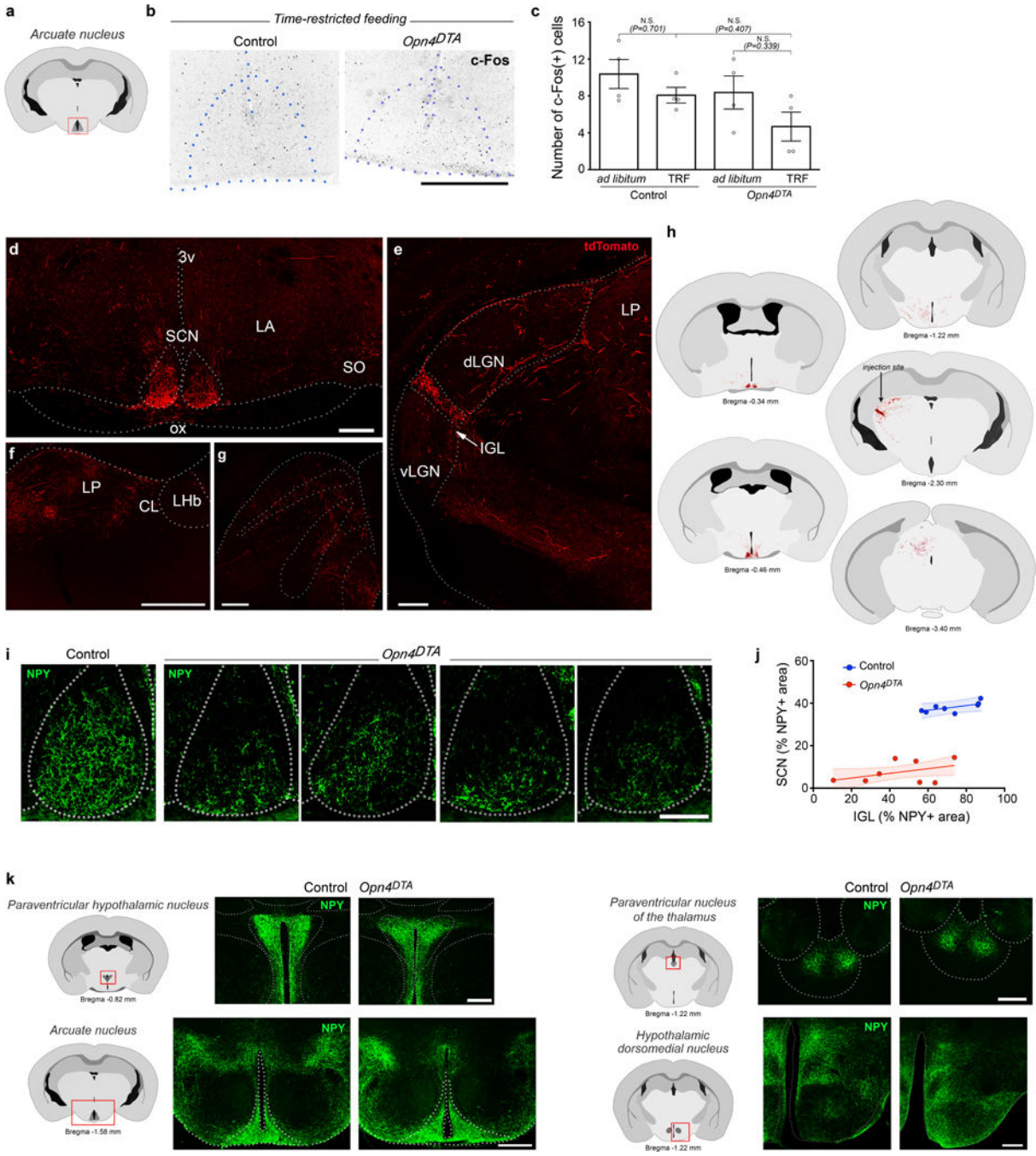

Extended data Fig. 2. Early ipRGC ablation causes alterations in the IGL^{NPY}-SCN circuit.

(**a** to **c**) c-Fos induction in the arcuate nucleus mediated by the expected food access. Mice were exposed to TRF and perfused on day 21st at the expected food time (right before food delivery). As controls, mice with food *ab libitum* were perfused at circadian time (CT) 12. All mice were housed under constant darkness (DD). The area analyzed is shown in a diagram of a representative coronal brain section (**a**). Representative images of control and *Opn4*^{DTA} mice exposed to TRF are shown (**b**); the number of c-Fos(+) cells in the arcuate nucleus was quantified (**c**). Data are mean ± SEM (n = 4 mice), Tukey's test, two tailed.

(**d** to **h)** Projection pattern of IGL^{NPY} cells. $NPY^{cre/+}$ mice were unilaterally injected in the IGL using a cre-dependent AAV-tdTomato (AAV2/9-phSyn1(S)-Flex-tdTomato-T2A-SynEGFP-WPRE). IGL^{NPY} neurons send dense and bilateral projections to the SCN (**d**), and to a least extend, unilateral projections to other brain targets, including the dorsal geniculate and dorsal thalamus (**e** and **f**), and the superior colliculus (**g**). The complete pattern of IGL^{NPY} projections is shown in a diagram of representative coronal brain sections (**h**). Three independent experiments were performed with similar results.

(**i**) Representative SCN sections obtained from control and $Opn4^{DTA}$ mice are shown. Drastic alterations in the pattern of NPY staining in the SCN were observed in $Opn4^{DTA}$ mice, compared to control mice.

(j) Correlation between NPY levels in somas and axonal terminals, measured in the IGL and SCN, respectively. Results obtained from Control and $Opn4^{DTA}$ mice are shown. *Pearson r* values were measured for both groups (Control = 0.728; $Opn4^{DTA}$ = 0.389). A linear regression was applied, and the comparison of slope fits was not significantly different (Slope ± SE: Control = 0.136 ± 0.052; $Opn4^{DTA}$ =0.100 ± 0.096). The asymptotic normal 95% confidence interval is shown for both groups. (n (Control) 7, ($Opn4^{DTA}$) 8 mice).

(**k**) Non-ipRGC innervated brain targets expressing NPY were studied in control and $Opn4^{DTA}$ mice. No obvious changes in NPY expression levels were observed in the paraventricular hypothalamic nucleus, arcuate nucleus, paraventricular nucleus of the thalamus, or hypothalamic dorsomedial nucleus. Three independent experiments were performed with similar results.

3v: third ventricle; ox: optic chiasm; SO: supraoptic nucleus; LA: lateroanterior hypothalamic nucleus; dLGN and vLGN: dorsal and ventral lateral geniculate, respectively; LP: lateral posterior thalamic nucleus; LHb: lateral habenula; CL: centrolateral nucleus of the thalamus.

Scale bar: 100 μm (b, i, k), 200 μm (d, f), 400 μm (e, g).

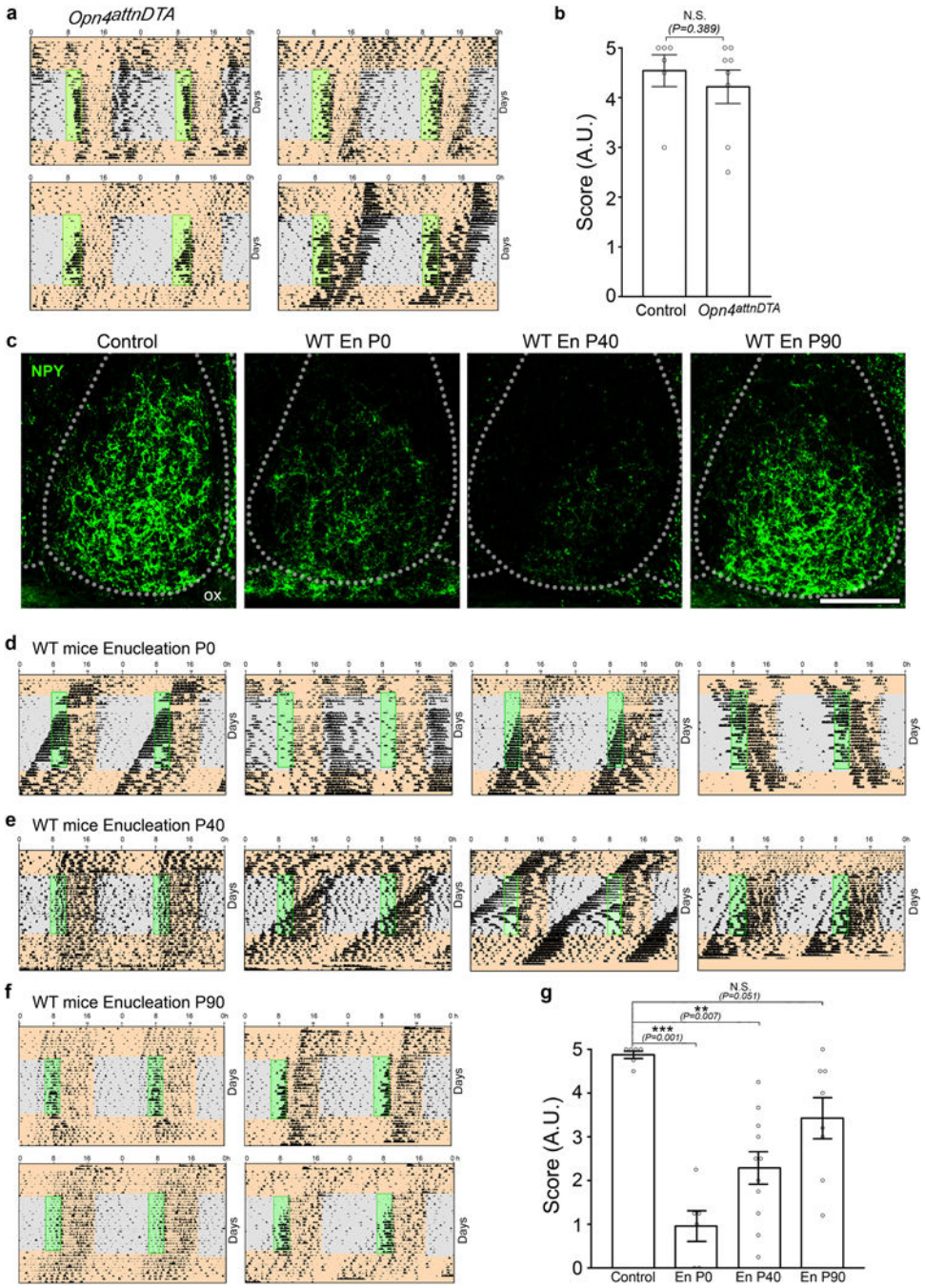

Extended data Fig. 3. ipRGCs influence the IGL-SCN circuit during early postnatal stages.

(**a** and **b**) Representative actograms obtained from *Opn4*^{attnnDTA} mice housed under TRF (**a**). A score analysis was performed for all actograms obtained (**b**). Data are mean ± SEM (n = (Control) 6, (*Opn4*^{attnDTA}) 8 mice), Student's t non-parametric (Mann-Whitney) test, two tailed.

(**c**) Representative coronal sections obtained from WT control and enucleated mice are shown. NPY(+) fibers were measured in the SCN area. Five independent experiments were performed with similar results.

(**d** to **g**) Representative actograms obtained from WT mice enucleated at P0 (**d**), P40 (**e**), or P90 (**f**) under TRF. A score analysis was performed for all actograms obtained (**g**). Data are mean ± SEM (n = (Control) 5, (EnP0) 6, (EnP40) 11, (EnP90) 8 mice), Student's t non-parametric (Mann-Whitney) test, two tailed.
Scale bar: 100 μm.

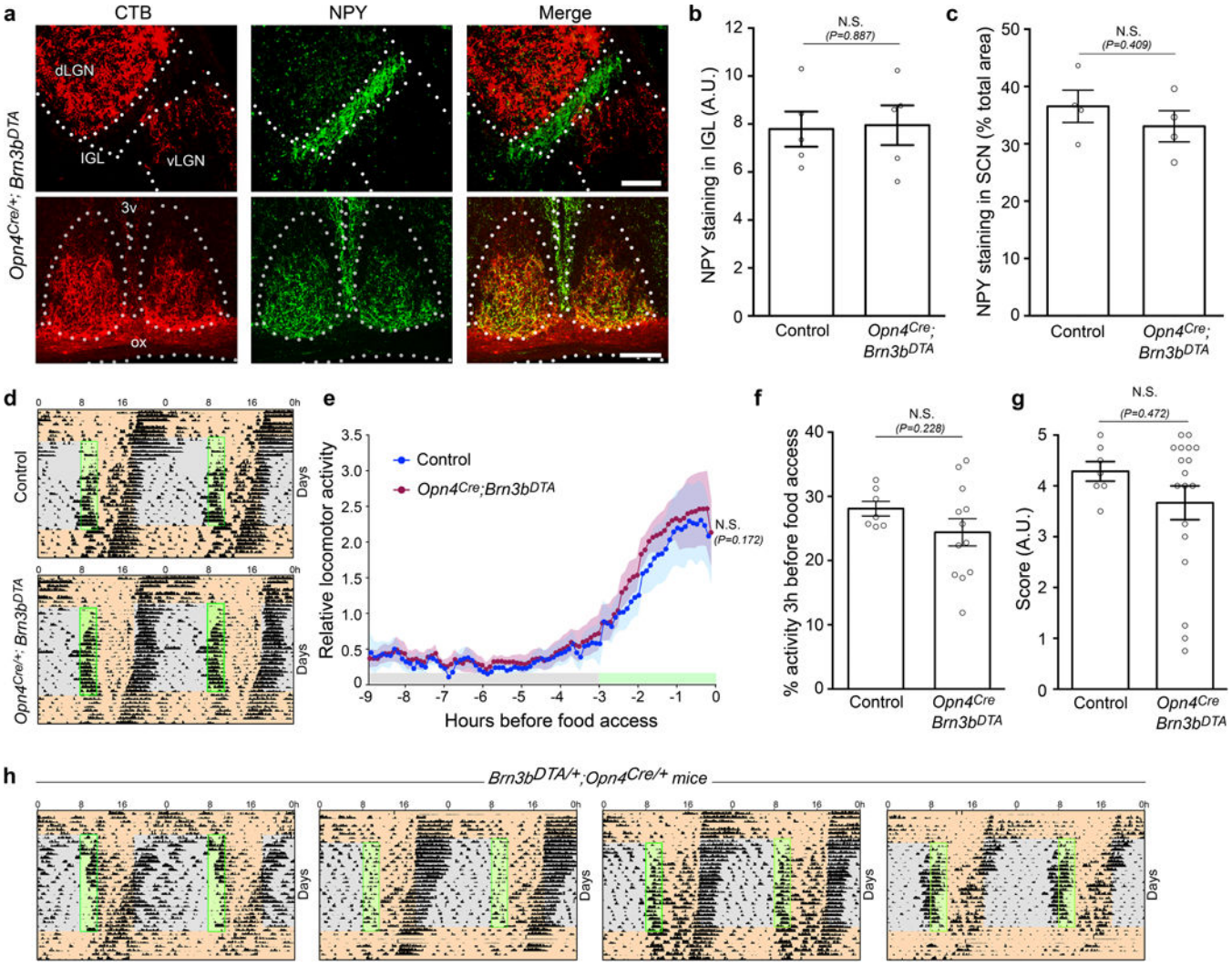

Extended data Fig. 4. Role of SCN-projecting ipRGCs in non-photic entrainment.

(**a** to **c**) Retinal innervation (CTB, red) and NPY staining (green) in the IGL and SCN in control and *Opn4*$^{Cre/+}$;*Brn3b*$^{DTA/+}$ mice. Representative coronal sections are shown (**a**). NPY staining in the IGL (**b**) and SCN (**c**) were analyzed in 3-month-old mice. Data are mean ± SEM (n = 5 mice), Student's t test, two-tailed.

(**d** to **h**) Control and *Opn4*$^{Cre/+}$;*Brn3b*$^{DTA/+}$ mice were exposed to TRF. Representative actograms are shown (**d**). The locomotor activity before food access (**e**) and the food-anticipatory activity (**f**) were measured. Data are mean ± SEM (n = (Control) 7, (*Opn4*$^{Cre/+}$;*Brn3b*$^{DTA/+}$) 12 mice), by Student's t test, two-tailed. Finally, a score analysis was performed for all actograms obtained (**g**). Data are mean ± SEM (n = (Control) 7, (*Opn4*$^{Cre/+}$;*Brn3b*$^{DTA/+}$) 18 mice), by Student's t non-parametric (Mann-Whitney) test, two tailed. Representative actograms obtained from *Opn4*$^{Cre/+}$;*Brn3b*$^{DTA/+}$ mice under TRF (**h**). Scale bar: 100 μm (a, SCN); 200 μm (a, IGL).

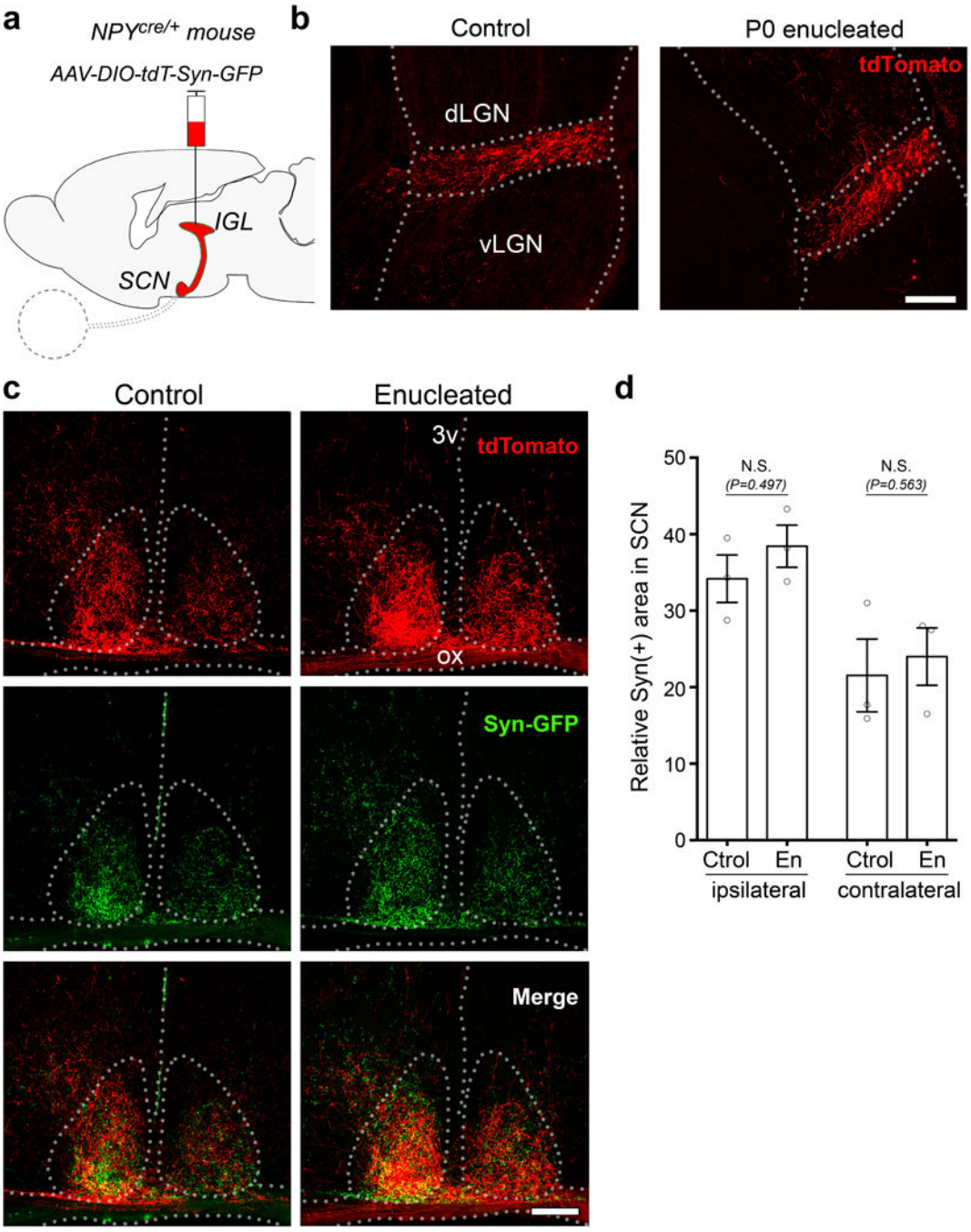

Extended data Fig. 5. Early ipRGC input to SCN influences afferent IGL^{NPY} projections.

(**a**) NPY$^{cre/+}$ mice, with or without bilateral enucleation at P0, were injected in the IGL with a cre-dependent AAV-tdT-Syn-GFP.

(**b**) Representative IGL injections in adult control and P0 enucleated NPY$^{cre/+}$ mice are shown. Three independent experiments were performed with similar results.

(**c-d**) Axonal projections (tdT, red) from IGL^{NPY} cells and their synaptic terminals (syn-GFP, green) are shown (**c**). IGL^{NPY} synaptic terminals were quantified (**d**). Data are mean ±

SEM (n = 3 mice), Student's t test, two-tailed. dLGN and vLGN: dorsal and ventral lateral geniculate, respectively.
Scale bar: 200 μm (b); 100 μm (c).

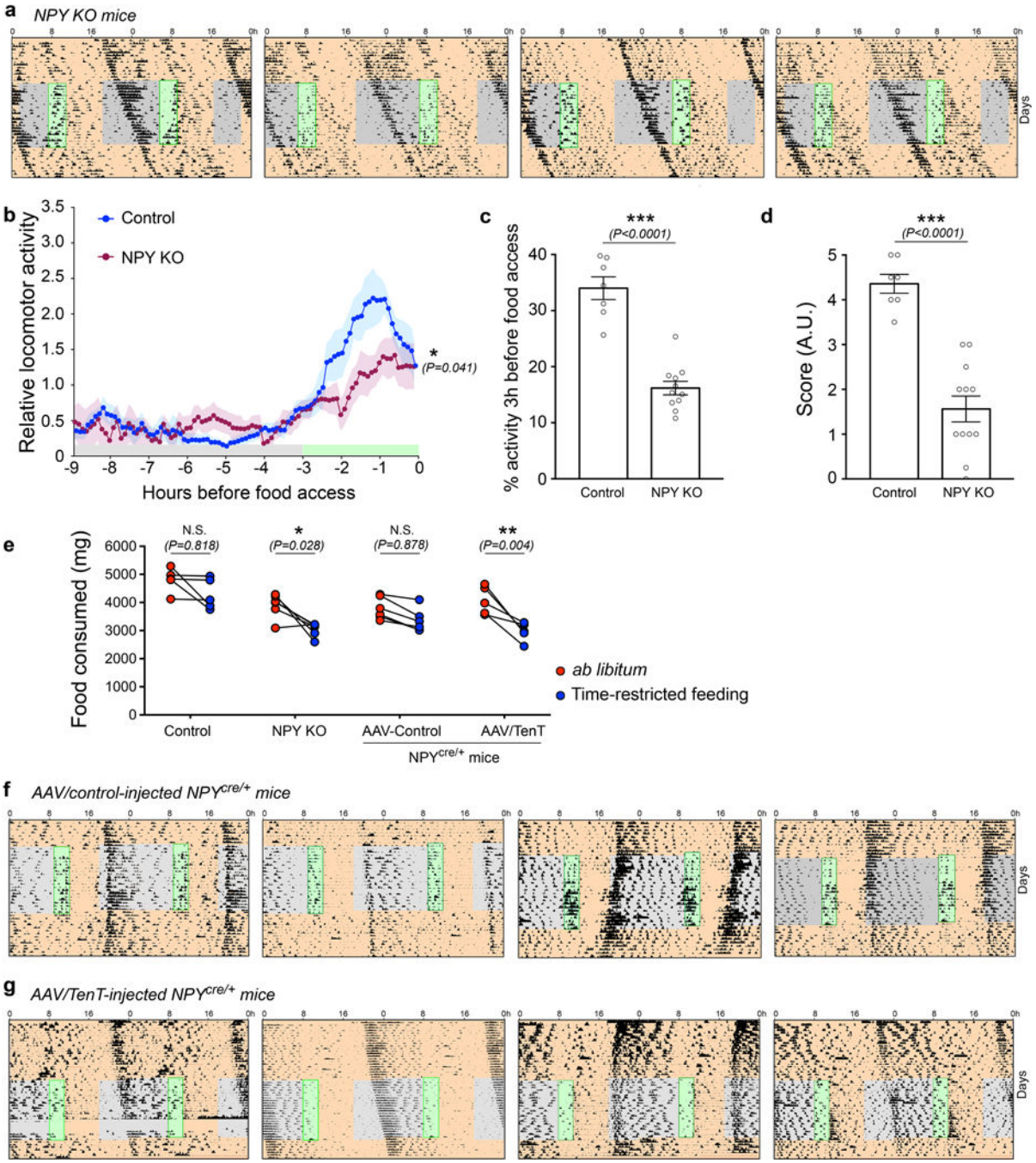

Extended data Fig. 6. NPY signaling in the IGL-SCN circuit controls non-photic entrainment.

(**a** to **d**) Representative actograms obtained from NPY KO (*NPY*$^{cre/cre}$) mice exposed to TRF are shown (**a**). The locomotor activity before (9-hour) food access (**b**), and the food-anticipatory activity (**c**) were measured for control and NPY KO mice. Data are mean ± SEM (n = (Control) 7, (NPY KO) 11 mice), Student's t test, two-tailed. Additionally, a score analysis was performed for all actograms obtained (**d**). Data are mean ± SEM (n = (Control) 7, (NPY KO) 11 mice), Student's t non-parametric (Mann-Whitney) test, two tailed. In

addition, a second mouse line (*NPY*^{tm1Rpa}) was used to evaluate the effects of NPY ablation. Results obtained from both NPY KO mouse lines were indistinguishable (data not shown). (**e**) The daily total amount of food consumed (during food *ad libitum* and TRF) was measured in control, NPY KO (*NPY*$^{cre/cre}$), and *NPY*$^{cre/+}$ mice bilaterally injected in the IGL with AAV/control (AAV5/Syn-DIO-hChR2(H134R)-EGFP-WPRE-HGHpA) or AAV/TenT (pAAV5/CMV-DIO-eGFP-2A-TeNT). Under free-running conditions (DD and food *ad libitum*), the amount of food consumed between control and NPY KO ($P = 0.0267$), as well as control and *NPY*$^{cre/+}$ mice ($P = 0.008$) were significantly different. Data are mean ± SEM (n = 5 mice), two-way ANOVA, followed by Sidak's multiple comparisons test. (**f** to **g**) Representative actograms obtained from AAV/control (**f**) or AAV/TenT (**g**) injected *NPY*$^{cre/+}$ mice exposed to TRF are shown.

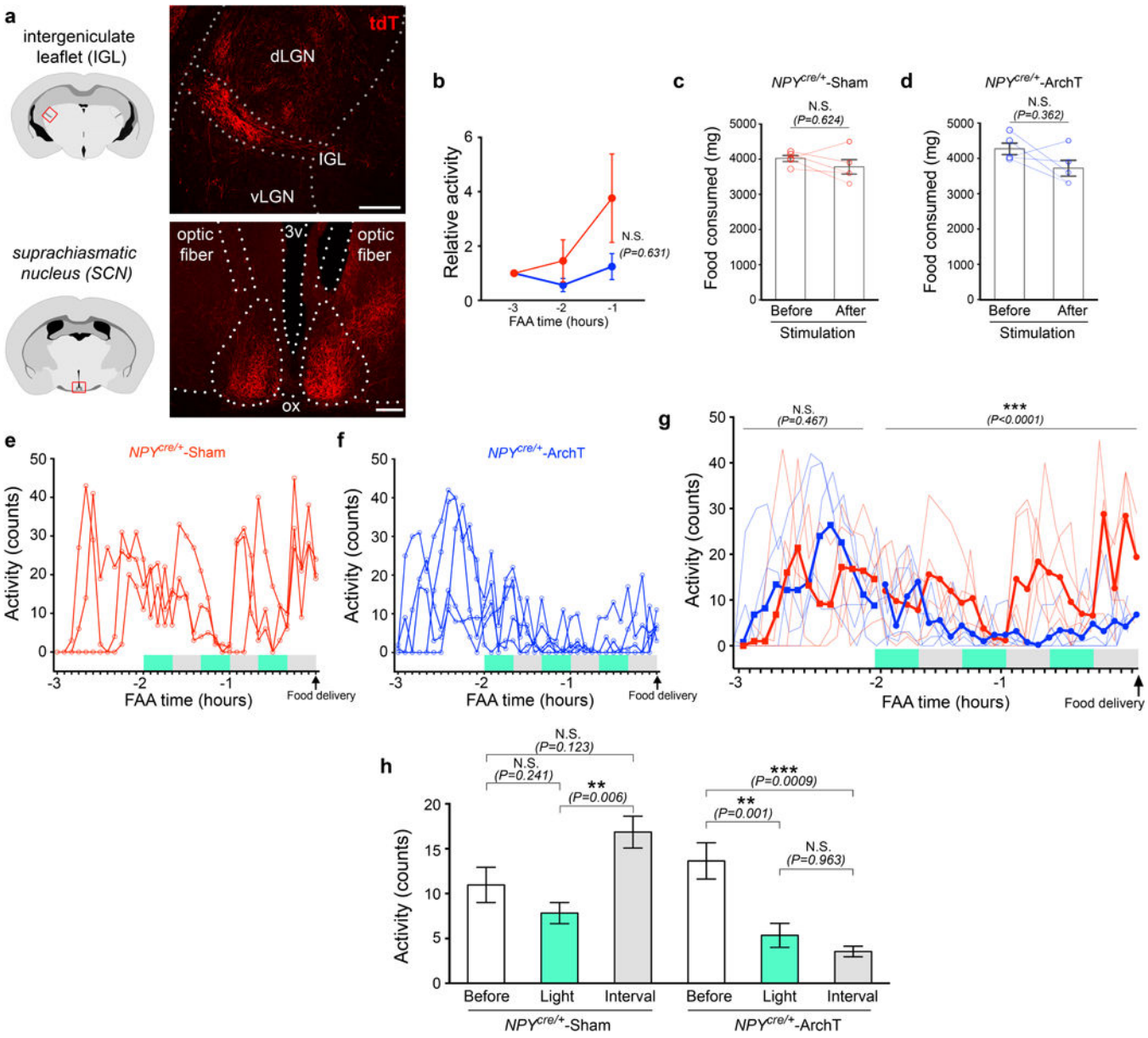

Extended data Fig. 7. Neural silencing of IGL^{NPY}-SCN circuit.

(**a**) Sites of injections (IGL) and optical fiber implantation (SCN) were confirmed at the end of the experiments.

(**b**) *NPY$^{cre/+}$-sham* (AAV/DIO-tdTomato) and *NPY$^{cre/+}$-ArchT* (AAV5/DIO-ArchT-tdTomato) mice were housed under TRF for 3 weeks and the locomotor activity was then measured for 3 hours before food access. Results are shown as relative activity (total counts per hour) during food-anticipatory activity (FAA). Data are mean ± SEM (n = 5 mice), two-way ANOVA, followed by Sidak's multiple comparisons test.

(**c** and **d**) Food consumed during TRF. The average of food consumed was measured for 10 days before optogenetic stimulation (before); the amount of food consumed the day of neural silencing was also measured (after) for both groups of mice. Data are mean ± SEM (n = 5 mice), paired Student's t test, two tailed.

(**e** to **h**) Locomotor activity was quantified (5 min bin) starting 3 hours before food access. Two hours before food access, neural silencing was induced by applying 3 pulses of light, 20 min each (shown in green), with 20 min intervals (shown in grey). Results of locomotor activity obtained for all $NPY^{cre/+}$-*sham* (**e**) and $NPY^{cre/+}$-*ArchT* (**f**) mice are shown. The average of results in also shown (**g**); similar food-anticipatory activity was observed in both groups without optical stimulation, whereas a significant reduction in locomotor activity was found in $NPY^{cre/+}$-*ArchT* mice during optogenetic stimulation. Data are mean ± SEM (n = 5 mice), two-way ANOVA, followed by Sidak's multiple comparisons test. For $NPY^{cre/+}$-*sham* mice, no changes in total activity were observed during light stimulation (light), or intervals between light pulses (interval), compared with activity measured during the first hour of food-anticipatory activity (before) (**h**). We observed a significant reduction in activity with light stimulation compared with intervals periods, suggesting that the light could have a direct masking effect on animal activity. However, the activity was fully recovered immediately after stimulation. Remarkably, $NPY^{cre/+}$-*ArchT* mice displayed similar and reduced activity for both stimulation and intervals periods, compared with activity displayed before optogenetic stimulation. Data are mean ± SEM (n = 5 mice), Tukey's test, two tailed. dLGN and vLGN: dorsal and ventral lateral geniculate, respectively; 3v: third ventricle; ox: optic chiasm.
Scale bar: 100 μm (a, SCN); 200 μm (a, IGL)

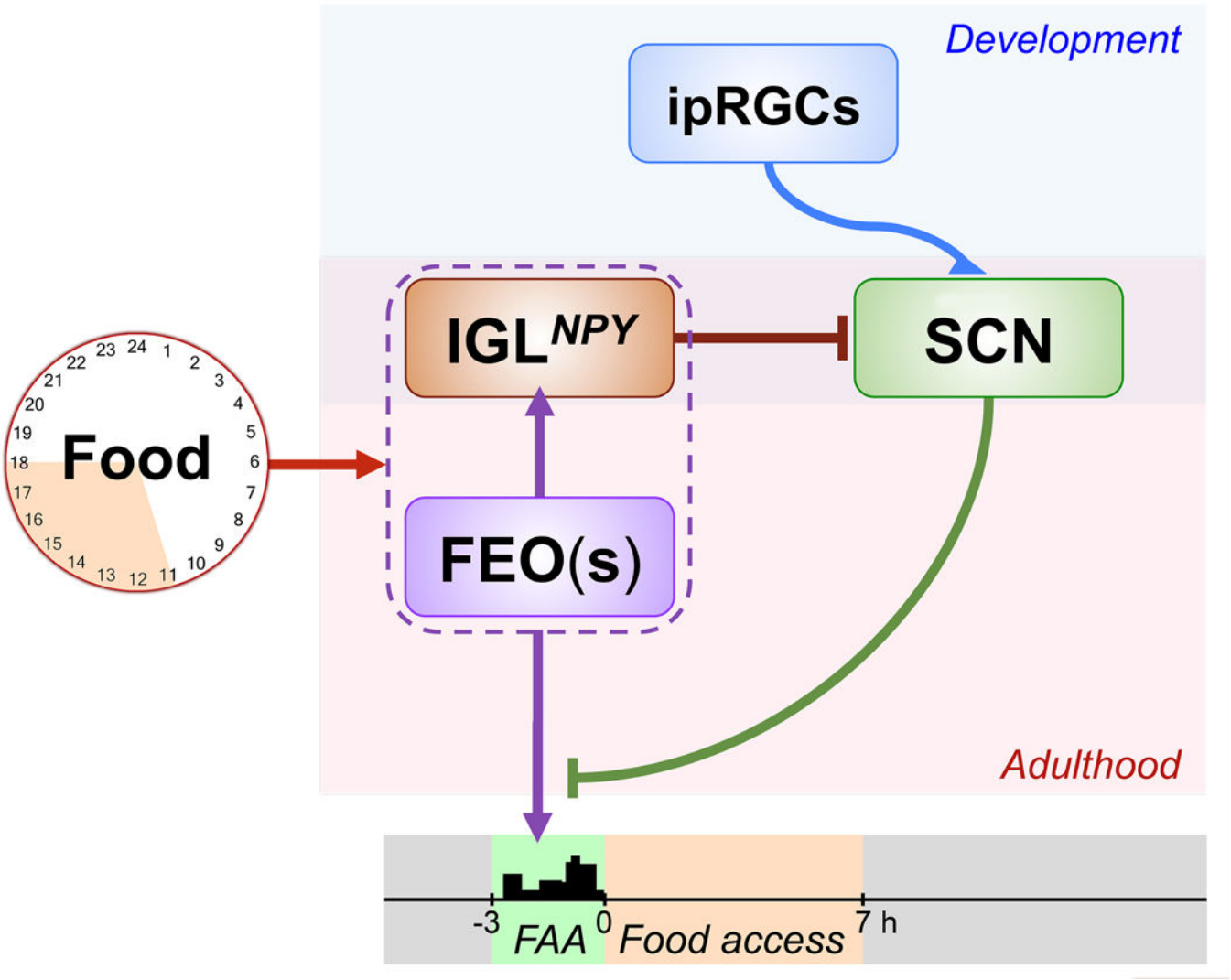

Extended data Fig. 8. Putative model for the circuit driving circadian food-anticipatory activity

Time-restricted access to food constitutes a strong environmental cue that causes the alignment of the circadian system to feeding schedules, driving food-anticipatory activity (FAA) that precedes the expected meal. The current view in the field is that a widespread system, referred to as food-entrainable oscillators (FEOs), controls the physiological and behavioral responses to TRF. Among all the candidates, are areas of the hypothalamus, such as the paraventricular nucleus (PVN), ventromedial hypothalamic nucleus (VHM), dorsomedial hypothalamic nucleus (DHM), and arcuate nucleus, thalamic areas, such as the paraventricular thalamus (PVT) and the intergeniculate leaflet (IGL), the brainstem, including the dorsal raphe nucleus (DR), and parabrachial nucleus (PBN), other brain regions as the dorsal striatum (Str), infralimbic cortex (ILC), nucleus accumbens (NAc), cerebellum (Cb), as well as peripheral targets, such as the gastrointestinal system (Gi). In the present study, we have delineated a brain circuit, IGL^{NPY}-SCN, critical for driving FAA in adult mice. Remarkably, the functional assembly of this circuit requires retinal ipRGC innervation to SCN during a critical window. The proposed model suggests a

crosstalk between FEO(s) and the IGL, where IGL neurons act as a node of connection between the FEOs and the central pacemaker (SCN). Under TRF, inhibitory signals from IGL^{NPY} neurons modulate the SCN function, causing a reduced firing activity, and therefore allowing FEO(s) signals to drive robust food anticipatory activity.

The IGL could also be part of the FEO(s), as previously suggested. IGL^{NPY} neurons send projections to several brain regions, and therefore, the role of any of these non-SCN projections in modulating FAA should not be excluded. How feeding-related stimuli modulate the FEO(s), and possibly IGL, are still unknown. Different humoral signals, such as ghrelin and insulin, are strong candidates for modulating the FEO(s) and IGL.

Extended data Table 1.

Systemic metabolic measurements in control and *Opn4*^{DTA} mice housed under free-running or time-restricted feeding.

	Control			***Opn4*^{DTA}**		
	Food ad libitum		**Ctrol-TRF**	***Food ad libitum***		**DTA-TRF**
	Ctrol-CT2	**Ctrol-CT14**		**DTA-CT2**	**DTA-CT14**	
Ghrelin (ng/mL)	2.25 ± 0.30	2.04 ± 0.16 *N.S. vs. Ctrol-CT2*	4.78 ± 0.62 ***(P=0.0015) vs: Ctrol-CT2* ***(P=0.0035) vs. Ctrot-CT14*	2.89 ± 0.41 *N.S. vs. Ctrol-CT2*	2.06 ± 0.31 *N.S. vs. DTA-CT2* *N.S. vs. Ctrol-CT14*	2.84 ± 0.44 *N.S. vs. DTA-CT2* *N.S. vs. DTA-CT14* **(P=0.0157) vs. Ctrol-TRF*
Insulin (ng/mL)	0.68 ± 0.09	0.92 ± 0.20 *N.S. vs. Ctrol-CT2*	0.47 ± 0.08 *N.S. vs. Ctrol-CT2* *N.S. vs. Ctrol-CT14*	0.91 ± 0.13 *N.S. vs. Ctrol-CT2*	0.95 ± 0.20 *N.S. vs. DTA-CT2* *N.S. vs. Ctrol-CT14*	0.51 ± 0.09 *N.S. vs. DTA-CT2* *N.S. vs. DTA-CT14* *N.S. vs Ctrol-TRF*
Leptin (ng/mL)	1.88 ± 0.39	3.35 ± 0.73 *N.S. vs. Ctrol-CT2*	3.73 ± 0.57 *N.S. vs. Ctrol-CT2* *N.S. vs. Ctrol-CT14*	3.37 ± 0.73 *N.S. vs. Ctrol-CT2*	3.99 ± 1.20 *N.S. vs. DTA-CT2* *N.S. vs. Ctrol-CT14*	4.77 ± 0.96 *N.S. vs. DTA-CT2* *N.S. vs. DTA-CT14* *N.S. vs. Ctrol-TRF*
Glucose (ng/mL)	104.0 ± 3.9	106.4 ± 2.6 *N.S. vs. Ctrol-CT2*	105.3 ± 4.2 *N.S. vs. Ctrol-CT2* *N.S. vs. Ctrol-CT14*	125.7 ± 9.5 *N.S. vs. Ctrol-CT2*	104.4 ± 6.2 *N.S. vs. DTA-CT2* *N.S. vs. Ctrol-CT14*	96.5 ± 8.8 *N.S. vs. DTA-CT2* *N.S. vs. DTA-CT14* *N.S. vs. Ctrol-TRF*

Blood samples were collected at circadian time (CT) 2 and 14 (inactive/active phase, respectively) from mice housed under free-running conditions (food *ad libitum*) or TRF (day 21st, right before food access).

Ghrelin (total), insulin, leptin, and glucose levels (ng/mL) were measured for all samples.

Data are mean ± SEM (n = 13 mice).

$^{*}P < 0.05$,

$^{**}P < 0.01$,

Tukey's test, two tailed.

Ctrol: Control mice; DTA: *Opn4*^{DTA} mice; CT: circadian time; TRF: time-restricted feeding

Supplementary Material

Refer to Web version on PubMed Central for supplementary material.

ACKNOWLEDGMENTS

We would like to thank the members of the SLCR at NIMH, the Johns Hopkins Biology Mouse Tri-Lab, and Maria E. Mercau for helpful discussions. We would also wish to thank Oksana Gavrilova and the NIDDK Mouse Metabolism Core for their skillful technical assistance, and Victoria Acosta-Rodríguez for her assistance with the programmable feeders.

This work was supported by the NIH (GM076430, EY027202), the generous contributions of the PEW Charitable Trusts (to D.C.F.), and the intramural research at the National Institute of Mental Health (ZIAMH002964-02).

REFERENCES

1. Golombek DA & Rosenstein RE Physiology of Circadian Entrainment. Physiol. Rev. 90, 1063–1102 (2010). [PubMed: 20664079]
2. Cappe C, Rouiller EM & Barone P Cortical and Thalamic Pathways for Multisensory and Sensorimotor Interplay. (2012). at <http://www.ncbi.nlm.nih.gov/books/NBK92866/>
3. Mahoney JR et al. Keeping in touch with the visual system: spatial alignment and multisensory integration of visual-somatosensory inputs. Front. Psychol. 6, 1068 (2015). [PubMed: 26300797]
4. Güler AD et al. Melanopsin cells are the principal conduits for rod-cone input to non-image-forming vision. Nature 453, 102–5 (2008). [PubMed: 18432195]
5. Hattar S, Liao HW, Takao M, Berson DM & Yau KW Melanopsin-containing retinal ganglion cells: architecture, projections, and intrinsic photosensitivity. Science 295, 1065–70 (2002). [PubMed: 11834834]
6. Berson DM, Dunn FA & Takao M Phototransduction by retinal ganglion cells that set the circadian clock. Science 295, 1070–3 (2002). [PubMed: 11834835]
7. Saderi N et al. The NPY intergeniculate leaflet projections to the suprachiasmatic nucleus transmit metabolic conditions. Neuroscience 246, 291–300 (2013). [PubMed: 23680526]
8. Moore RY & Card JP Intergeniculate leaflet: An anatomically and functionally distinct subdivision of the lateral geniculate complex. J. Comp. Neurol. 344, 403–430 (1994). [PubMed: 8063960]
9. Morin LP Neuroanatomy of the extended circadian rhythm system. Exp. Neurol. 243, 4–20 (2013). [PubMed: 22766204]
10. Wams EJ, Riede SJ, van der Laan I, ten Bulte T & Hut RA in Biological Timekeeping: Clocks, Rhythms and Behaviour 395–404 (Springer India, 2017). doi:10.1007/978–81-322–3688-7_18
11. Chew KS et al. A subset of iprgcs regulates both maturation of the circadian clock and segregation of retinogeniculate projections in mice. Elife 6, (2017).
12. Mistlberger RE Food-anticipatory circadian rhythms: concepts and methods. Eur. J. Neurosci. 30, 1718–1729 (2009). [PubMed: 19878279]
13. Acosta-Galvan G et al. Interaction between hypothalamic dorsomedial nucleus and the suprachiasmatic nucleus determines intensity of food anticipatory behavior. Proc. Natl. Acad. Sci. 108, 5813–5818 (2011). [PubMed: 21402951]
14. Patton DF et al. Photic and Pineal Modulation of Food Anticipatory Circadian Activity Rhythms in Rodents. PLoS One 8, e81588 (2013). [PubMed: 24324709]
15. Nakazato M et al. A role for ghrelin in the central regulation of feeding. Nature 409, 194–198 (2001). [PubMed: 11196643]
16. Camiña JP et al. Regulation of Ghrelin Secretion and Action. Endocrine 22, 5–12 (2003). [PubMed: 14610293]
17. Blum ID, Waddington Lamont E, Rodrigues T & Abizaid A Isolating Neural Correlates of the Pacemaker for Food Anticipation. PLoS One 7, e36117 (2012). [PubMed: 22558352]
18. Glass JD, Guinn J, Kaur G & Francl JM On the intrinsic regulation of neuropeptide Y release in the mammalian suprachiasmatic nucleus circadian clock. Eur. J. Neurosci. 31, 1117–1126 (2010). [PubMed: 20377624]
19. Andermann ML & Lowell BB Toward a Wiring Diagram Understanding of Appetite Control. Neuron 95, 757–778 (2017). [PubMed: 28817798]

20. Chen S-K, Badea TC & Hattar S Photoentrainment and pupillary light reflex are mediated by distinct populations of ipRGCs. Nature 476, 92–5 (2011). [PubMed: 21765429]
21. Fernandez DC et al. Light Affects Mood and Learning through Distinct Retina-Brain Pathways. Cell 175, 71–84.e18 (2018). [PubMed: 30173913]
22. Sindelar DK, Palmiter RD, Woods SC & Schwartz MW Attenuated feeding responses to circadian and palatability cues in mice lacking neuropeptide Y. Peptides 26, 2597–2602 (2005). [PubMed: 15923061]
23. May PJ The mammalian superior colliculus: Laminar structure and connections. Progress in Brain Research 151, 321–378 (2006). [PubMed: 16221594]
24. Gandhi NJ & Katnani HA Motor functions of the superior colliculus. Annu. Rev. Neurosci. 34, 205–31 (2011). [PubMed: 21456962]
25. Stein BE, Stanford TR & Rowland BA Development of multisensory integration from the perspective of the individual neuron. Nat. Rev. Neurosci. 15, 520–35 (2014). [PubMed: 25158358]
26. Mundiñano IC & Martínez-Millán L Somatosensory cross-modal plasticity in the superior colliculus of visually deafferented rats. Neuroscience 165, 1457–70 (2010). [PubMed: 19932888]
27. Waterson MJ & Horvath TL Neuronal Regulation of Energy Homeostasis: Beyond the Hypothalamus and Feeding. Cell Metab. 22, 962–970 (2015). [PubMed: 26603190]
28. Sheng Z, Santiago AM, Thomas MP & Routh VH Metabolic regulation of lateral hypothalamic glucose-inhibited orexin neurons may influence midbrain reward neurocircuitry. Mol. Cell. Neurosci. 62, 30–41 (2014). [PubMed: 25107627]
29. Azevedo EP et al. A Role of Drd2 Hippocampal Neurons in Context-Dependent Food Intake. Neuron 0, (2019).
30. Challet E The circadian regulation of food intake. Nat. Rev. Endocrinol. (2019). doi:10.1038/s41574–019-0210-x
31. Pendergast JS & Yamazaki S The Mysterious Food-Entrainable Oscillator: Insights from Mutant and Engineered Mouse Models. J. Biol. Rhythms 33, 458–474 (2018). [PubMed: 30033846]
32. Acosta-Rodríguez VA, de Groot MHM, Rijo-Ferreira F, Green CB & Takahashi JS Mice under Caloric Restriction Self-Impose a Temporal Restriction of Food Intake as Revealed by an Automated Feeder System. Cell Metab. 26, 267–277.e2 (2017). [PubMed: 28683292]
33. Franklin KBJ & Paxinos G Paxinos and Franklin's The mouse brain in stereotaxic coordinates.
34. Charan J & Kantharia N How to calculate sample size in animal studies? J. Pharmacol. Pharmacother. 4, 303 (2013). [PubMed: 24250214]
35. Faul F, Erdfelder E, Lang A-G & Buchner A G*Power 3: A flexible statistical power analysis program for the social, behavioral, and biomedical sciences. Behav. Res. Methods 39, 175–191 (2007). [PubMed: 17695343]

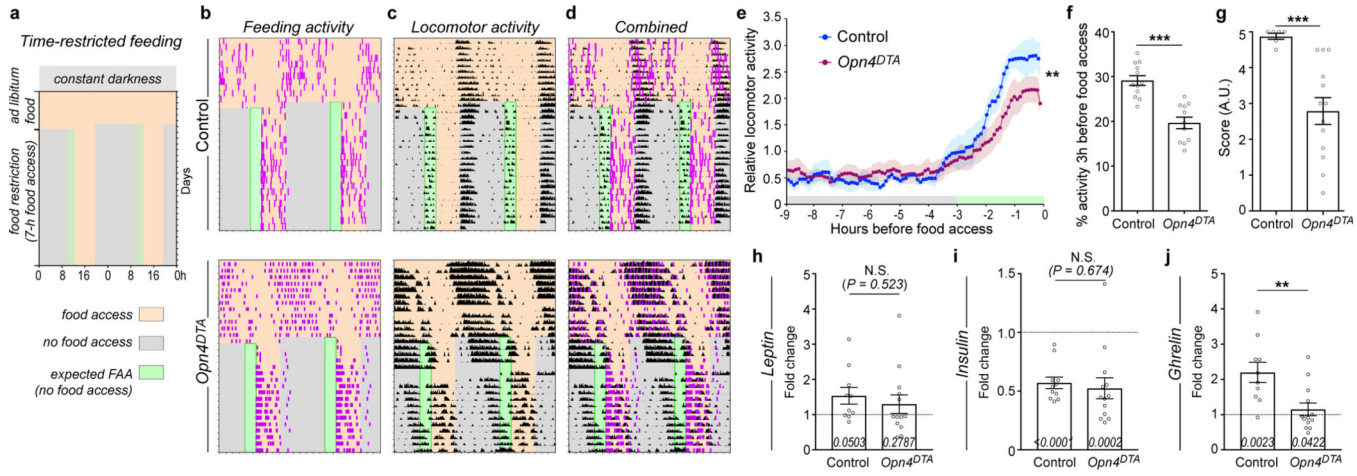

Fig. 1. Early ipRGC ablation affects circadian entrainment to TRF.

(**a**) Schematic illustrating the TRF paradigm.

(**b** to **d**) Representative actograms for feeding (**b**), locomotor activity (**c**), and combined actograms (**d**), measured in 3-month-old control and *Opn4*^{DTA} mice.

(**e** and **f**) The locomotor activity before food access (**e**), and relative food-anticipatory activity (**f**) were measured as described in the methods section. Data are mean ± SEM (n = (Control) 12, (*Opn4*^{DTA}) 13 mice), ***$P = 0.0001$, **$P = 0.0042$, Student's t test, two-tailed.

(**g**) A score analysis was performed for all actograms obtained from control and *Opn4*^{DTA} mice as described in the methods section. Data are mean ± SEM (n = (Control) 12, (*Opn4*^{DTA}) 13 mice), ***$P = 0.003$, Student's t non-parametric (Mann-Whitney) test, two tailed.

(**h** to **j**) Hormonal signals were measured in control and *Opn4*^{DTA} mice. The levels of leptin (**h**), insulin (**i**), and total ghrelin (**j**) were measured. Data is expressed as hormone's levels during food restricted access relative to free-running conditions. Data are mean ± SEM (n = (Control) 10, (*Opn4*^{DTA}) 13 mice), **$P = 0.0038$, Student's t test, two-tailed. In addition, the statistical analysis versus a hypothetical value = 1 (dotted lines) was performed, and is shown per column; by one sample t test.

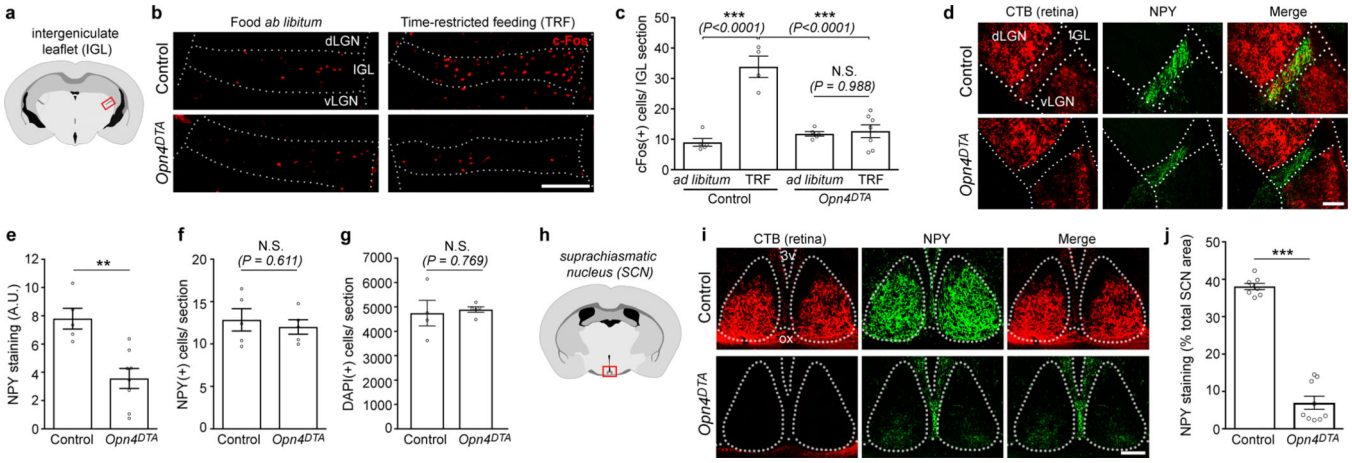

Fig. 2. Early ipRGC ablation alters the IGL^{NPY}-SCN connectivity.

(**a**) Schematic brain section highlighting the location of the IGL.

(**b** and **c**) Representative images showing cFos induction in IGL neurons in response to food ad libitum or TRF in 3-month-old control and *Opn4*^{DTA} mice (**b**) and quantified in (**c**). Data are mean ± SEM (n = 4 mice), ***$P < 0.001$, Tukey's test, two tailed.

(**d** to **g**) Morphological characterization of retinal innervation (CTB, red) and NPY staining (green) in the IGL in 3-month-old control and *Opn4*^{DTA} mice. Representative coronal sections are shown (**d**). The levels of NPY staining (**e**), number of NPY(+) somas (**f**) and DAPI(+) nuclei (**g**) were quantified. Data are mean ± SEM (n = (Control) 5, (*Opn4*^{DTA}) 8 mice), **$P = 0.0022$, Student's t test, two-tailed.

(**h**) Schematic brain section highlighting the location of the SCN.

(**i** and **j**) Retinal input to the SCN (CTB, red) and NPY from IGL (NPY, green). Representative images are shown (**i**). NPY staining in the SCN was quantified (**j**). Data are mean ± SEM (n = 8 mice), ***$P < 0.001$, Student's t test, two-tailed.

dLGN and vLGN: dorsal and ventral lateral geniculate, respectively; 3v: third ventricle; ox: optic chiasm. Scale bar: 100 μm (i); 200 μm (b, d).

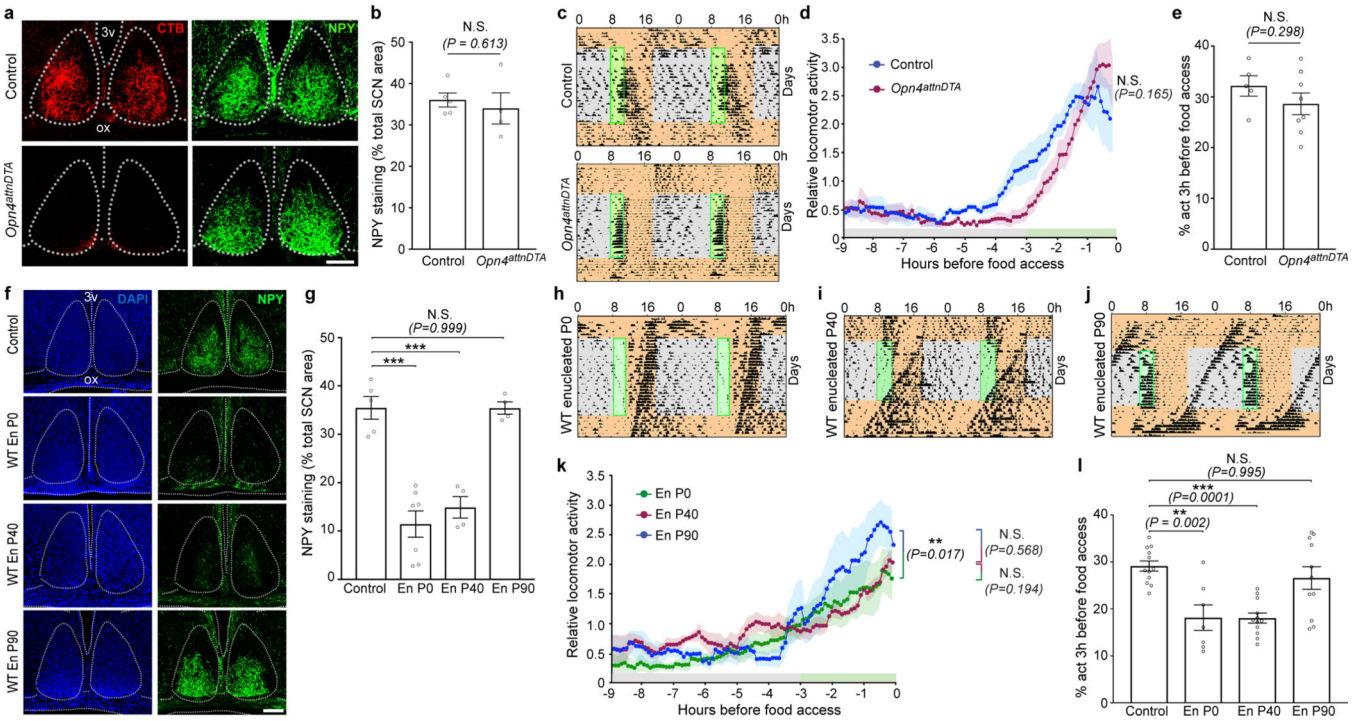

Fig. 3. Critical time window for IGL^{NPY}-SCN circuit assembly.

(**a** and **b**) Retinal (CTB, red) and IGL (NPY, green) innervation to SCN in 9-month-old control and *Opn4*^{attnDTA} mice. Representative SCN sections are shown (**a**). NPY staining was analyzed (**b**). Data are mean ± SEM (n = 5 mice), Student's t test, two-tailed.

(**c** to **e**) Locomotor activity was measured in control and *Opn4*^{attnDTA} mice exposed to TRF. Representative actograms are shown (**c**). The locomotor activity before food access (**d**), and the food-anticipatory activity (**e**) were measured. Data are mean ± SEM ((n = (Control) 5, (*Opn4*^{attnDTA}) 8 mice), Student's t test, two-tailed.

(**f** and **g**) IGL (NPY, green) innervation to SCN in 3 to 5-month-old in wild type (WT) control and enucleated (En) mice. Representative sections are shown (**f**). NPY staining in the SCN was analyzed (**g**). Data are mean ± SEM (n = (Control) 5, (EnP0) 7, (EnP40) 4, (EnP90) 5 mice); ***$P < 0.001$; by Tukey's test, two tailed.

(**h** to **l**) WT mice, enucleated at different stages, were exposed to TRF. Representative actograms are shown (**h-j**). The locomotor activity before food access (**k**) and the food-anticipatory activity (**l**) were measured in intact and enucleated mice. Data are mean ± SEM (n = (Control)11, (EnP0) 7, (EnP40) 12, (EnP90) 11 mice), Tukey's test, two tailed. Scale bar: 100 μm (a, f).

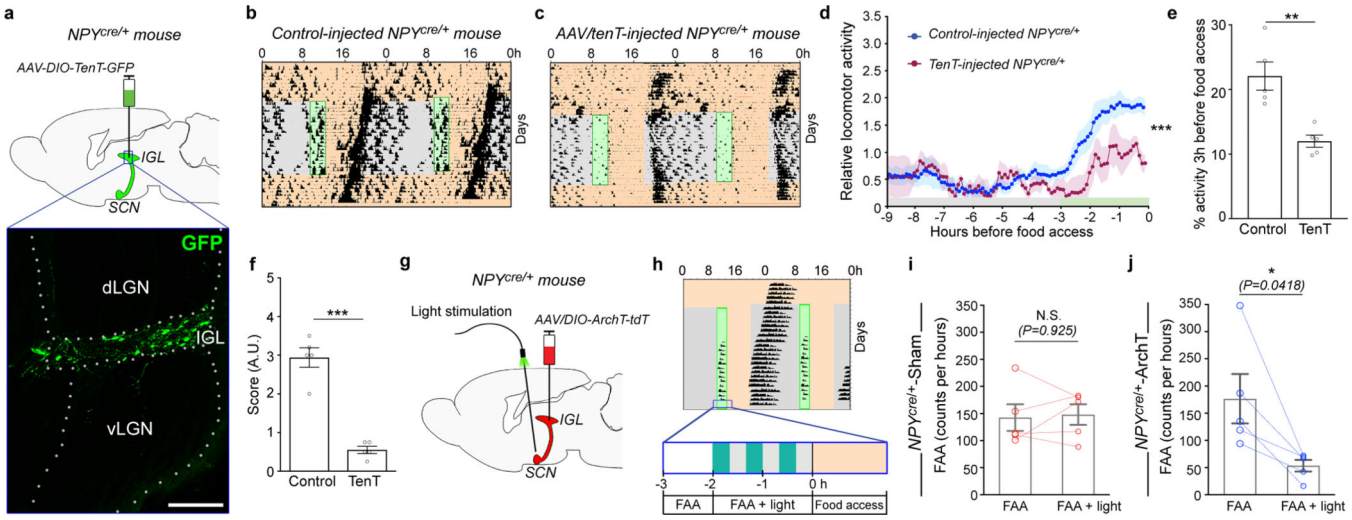

Fig. 4. NPY signaling in IGL-SCN circuit regulates entrainment to TRF.

(**a**) A cre-dependent AAV encoding tetanus toxin (TenT)-GFP was bilaterally injected into the IGL of 3-month-old *NPY*$^{cre/+}$ mice. Top, schematic. Bottom, injection site.

(**b** and **c**) Representative actograms obtained from an AAV/control (**b**) and AAV/TenT injected *NPY*$^{cre/+}$ (**c**) mice exposed to TRF.

(**d** to **f**) Locomotor activity before food access (**d**) and the food-anticipatory activity (**e**) were measured for control and *NPY*$^{cre/+}$ mice. Data are mean ± SEM (n = 5 mice), ***$P < 0.001$; **$P = 0.0029$, Student's t test, two-tailed. A score analysis was performed for all actograms obtained (**f**); data are mean ± SEM (n = 5 mice); ***$P = 0.0079$, Student's t non-parametric (Mann-Whitney) test, two-tailed.

(**g** to **h**) Optogenetic silencing of IGL^{NPY}-SCN circuit during food anticipatory activity (FAA). Schematic showing the AAV injections and cannula implantation (**g**). Schematic showing the optical stimulation protocol (**h**).

(**i** and **j**) Locomotor activity was measured for 3 hours (5 min bin) before food access in *NPY*$^{cre/+}$-sham (**i**) and *NPY*$^{cre/+}$-ArchT (**j**) mice exposed to TRF and optogenetic stimulation. Data was expressed as activity (total beam break counts per hour) measured during FAA, with or without optical stimulation. Data are mean ± SEM (n = 5 mice), *$P=0.0418$, paired Student's t test, two-tailed. Scale bar: 200 μm (a).